

Friction force microscopy investigations of potassium halide surfaces in ultrahigh vacuum: structure, friction and surface modification

R.W. Carpick*, Q. Dai**, D.F. Ogletree and M. Salmeron***

Materials Sciences Division, Lawrence Berkeley National Laboratory, University of California, Berkeley, CA 94720, USA

E-mail: salmeron@stm.lbl.gov

Received 12 July 1997; accepted 22 February 1998

Friction force microscopy measurements on the vacuum-cleaved (001) surfaces of KF, KCl and KBr have been carried out. All surfaces exhibit atomically flat terraces with monatomic steps aligned preferentially along low-index lattice directions. Stick-slip lateral forces with the lattice periodicity are observed on all surfaces. Tip-sample contact creates higher friction domains on the terraces of all three materials. The structure, topography and degree of friction force contrast of these domains is material dependent. The dependence of friction upon load generally does not coincide with the behavior expected for an elastic contact. We propose that the observed domains result from surface structural changes created by low load tip-sample contact on these relatively soft materials.

Keywords: force microscopy, alkali halide, KCl, KBr, KF, friction, wear, surface structure, nanotribology

1. Introduction

Atomic force microscopy (AFM) [1] provides the opportunity for high-resolution surface imaging. Furthermore, the measurement of lateral (frictional) forces with friction force microscopy (FFM) provides additional information regarding sample properties. However, the exact nature of the friction force interaction is not well understood [2]. Therefore, a systematic FFM study of related materials is desirable. We have studied a series of alkali halide single crystals where only the halogen ion is varied, namely KF, KCl and KBr. In general, alkali halides present relatively inert surfaces because of the closed-shell nature of the ionic bonding. Surfaces with atomically flat terraces can be prepared by cleavage in ultrahigh vacuum (UHV). An important difference amongst these materials is the different ionic radius of the anion. Almost all physical properties of these crystals (lattice constant, binding energy, elastic constants, etc.) vary from one material to the other in the same order as the anionic radii. Our goal is thus to examine whether observed frictional properties also vary in such a fashion.

Furthermore, we wish to investigate the surface properties of these materials. While the bulk properties of alkali halide materials have been extensively studied, surface properties have received less attention [3]. The strongly insulating nature of these materials renders electron spectroscopy methods, so common for surface science investigations, difficult to utilize. Specifically, the understand-

ing of surface defects of these materials remains minimal. With AFM, of course, sample conductivity is not required of samples under investigation.

2. Properties of potassium halides

Various relevant physical properties of KF, KCl and KBr are listed in table 1. The materials are listed in order of increasing anionic radius, which naturally corresponds to increasing atomic number. These materials all form the NaCl “rock-salt” structure, an fcc lattice with a basis of two atoms, the cation and anion. This structure is illustrated in figure 1. The highly ionic bonding character allows one to describe the ions as being packed like billiard balls whose radii are equal to the respective ionic radii. The F^- and K^+ ions possess similar radii [4] which leads to efficient packing and hence to the smallest nearest-neighbor distance of 0.267 nm. The larger Cl^- ion leads to a significantly larger nearest-neighbor distance of 0.315 nm. Br^- is slightly bigger than Cl^- and correspondingly KBr has a nearest-neighbor separation slightly larger than KCl of 0.330 nm. Similarly, the cohesive energies of KCl and KBr are nearly the same, with KCl slightly more strongly bound. The binding of KF is significantly stronger than both [5]. The elastic properties as exemplified by the Young’s modulus vary in a similar fashion [6]. Another important mechanical property is the yield strength. However, yield strength measurements are macroscopic in nature and thus invariably determined by dislocation behavior. The nanometer-sized contacts relevant for AFM may in fact possess yield strengths closer to the theoretical ideal [7] which for ionic materials, as with others, are proportional to the

* Currently at: Sandia National Laboratories, Mail Stop 1413, Albuquerque, NM 87185, USA.

** Currently at: IBM Corporation, 5600 Cottle Road, San Jose, CA 95193, USA.

*** To whom correspondence should be addressed.

Table 1
Properties of potassium halide crystals.

Sample	Cation (K^+) radius (nm)	Anion radius (nm)	Step height h (nm)	Lattice periodicity d (nm)	Cohesive energy (eV/ion pair)	Young's modulus (GPa)	Ideal strength (G/10–G/5) (GPa)
KF	0.133	0.136	0.267	0.378	8.2	60	1.3–2.6
KCl	0.133	0.181	0.315	0.445	7.2	39	0.63–1.3
KBr	0.133	0.195	0.330	0.467	6.9	33	0.53–1.0

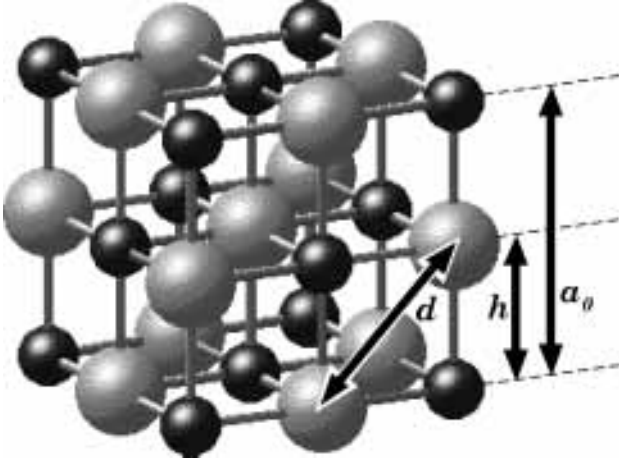


Figure 1. The rock-salt structure. Cations (small dark spheres) and anions (large light spheres) are arranged in an fcc lattice whose basis consists of a cation at $(0,0,0)$ and an anion at $(1/2,1/2,1/2)$. Indicated here are the dimensions of the conventional unit cell a_0 , the ion periodicity h ($= a_0/2$, which is the nearest-neighbor distance), and the lattice periodicity d ($= a_0/\sqrt{2}$) which is the nearest separation of equally-charged ions. The monatomic step height is equal to h . The values of d and h for the three materials studied are given in table 1. The ionic radii in the drawing are reduced from the actual values to display the structure more clearly.

elastic constants [8]. We expect, based on other work with nano-scale contacts [9], that the strength of these materials at the nanometer scale will vary accordingly. Specifically, the ideal yield strength of these materials is estimated to be within $G/10$ and $G/5$, where G is the shear modulus, and this range of values is indicated in table 1.

These samples also provide an interesting situation for the study of atomic-scale stick-slip behavior, detailed discussions of which are provided by Morita et al. [10] and Ogletree et al. [11]. In summary, the observed “lattice” in contact-mode AFM is due to the remarkable occurrence of lateral forces with atomic periodicity which occur despite the fact that the tip-sample contact area includes tens or even hundreds of unit cells. Thus, the nature of this periodic friction force remains unexplained. Usually the observed lateral forces on ionic materials possess the lattice periodicity [10,12,13], but lateral forces with half of the lattice periodicity were recently observed for an intermediate load range on a NaF sample [14]. Here we have an opportunity to observe the stick-slip phenomenon with the same tip for materials with varying ionic radii. Specifically, we wish to discover whether the similar radii of K^+ and F^- ions (see table 1) leads to distinct stick-slip behavior,

since a hard-shell model would suggest that both ions in the KF unit cell interact with the tip more equally than in the case of KCl or KBr.

In this study, we present results obtained in contact-mode AFM, where, as mentioned above, we do not expect to resolve individual atoms or point defects. By using continuum elastic theory to consider the tip-sample contact in the presence of adhesion, it is impossible, even at the lowest loads, to obtain a single-atom contact [15]. This is commonly revealed in AFM imaging by the lack of observation of point defects, as well as by the apparent width of atomic steps. True atomic resolution can only be obtained with AFM by using a non-contact dynamic force modulation technique [16], with which individual point defects were in fact observed for NaCl(001) in UHV [17].

3. Experimental section

For these experiments, we used commercially obtained high-purity optical grade single crystals of KBr and KCl [18], and a laboratory-grown high purity single crystal of KF [19]. Crystals were mounted with epoxy into a sample holder. Once in UHV, crystals were cleaved using a knife-edge, producing an optically flat (001) plane. All measurements were performed at room temperature with the chamber pressure below 5×10^{-10} Torr. The same silicon nitride cantilever was used for all experiments [20]. The force constant of the cantilever was estimated to be 0.11 N/m, derived from scanning electron microscope measurements of lever dimensions combined with elastic theory calculations [21]. The relative lateral force to normal force sensitivity ratio was experimentally determined using the “wedge” calibration technique [21]. The UHV AFM used for these experiments is described in detail elsewhere [22]. A nanometer scale profile of the tip was obtained by scanning sharp surface features on a SrTiO₃(305) sample [23]; this tip imaging technique has been described elsewhere [24]. The tip shape was confirmed to be essentially parabolic with a curvature radius of 45 ± 5 nm.

Two types of data are presented in this paper. Images were obtained in the usual topographic mode by maintaining a constant applied normal force, while simultaneously recording the lateral force signal. Friction vs. load plots were obtained by plotting the average difference in bi-directional lateral force signals during a 10 nm lateral scan

on an atomically flat terrace for a series of loads, as described elsewhere [25]. Loads are reported with respect to zero lever deflection, i.e., zero net force acting on the lever. Thus, negative loads correspond to measurements in the tensile regime, and positive loads correspond to measurements in the compressive regime.

4. Results

4.1. Sample topography

Images were acquired as soon as 20 min after cleavage of the crystals. Surface structures (i.e., steps) remained stable over periods of several hours (changes to the surface induced by tip-sample contact will be discussed below).

In all cases, vacuum cleavage produces flat terraces with lateral dimensions of typically several hundreds of nanometers. Many steps are observed and are overwhelmingly monatomic steps, i.e., the step height $h = a_0/2$ where a_0 is the conventional unit cell size. This corresponds to a single (001) slab of material. The steps are oriented predominantly, but not exclusively, along the [100] and [010] lattice directions (see figure 2). We determined this by observing the relative alignment of these steps to be 90° , and comparing their orientation to the direction of rows in the lateral force stick-slip images which are discussed in the next section. The direction of these steps is also consistent with the macroscopic orientation of the crystal in the sample holder. We refer to these steps as “low index steps”. Figure 2 is an example from the KBr surface. Along with low index steps we also see two kinked steps oriented in a unique direction. The low index steps are seen to cross each other as well as the kinked steps. The low index steps are most likely the result of edge or screw dislocations that are exposed by cleavage. It is energetically favorable for dislocation features to run along low index directions.

Highly stepped regions are observed as well. An example from the KF surface is shown in figure 4. Numerous pointed terraces with relatively consistent opening angles are present. These regions may be the result of the interaction between preexisting dislocations and the cleavage process. Areas with large terraces were also observed on this sample.

The steps observed on these surfaces in vacuum are markedly different than those observed on surfaces imaged in ambient conditions. At various humidities, steps on rock-salt crystal surfaces are observed to have rounded shapes [26]. Increased mobility of surface ions due to hydration allows step flow to occur, leading to an equilibrium configuration.

4.2. Atomic lattice resolution

Atomic lattice resolution lateral force images of all three materials were obtained. An example from KF is presented in figure 5. The lateral force images display periodic stick-slip behavior with periodicities of 0.39 ± 0.02 nm for KF,

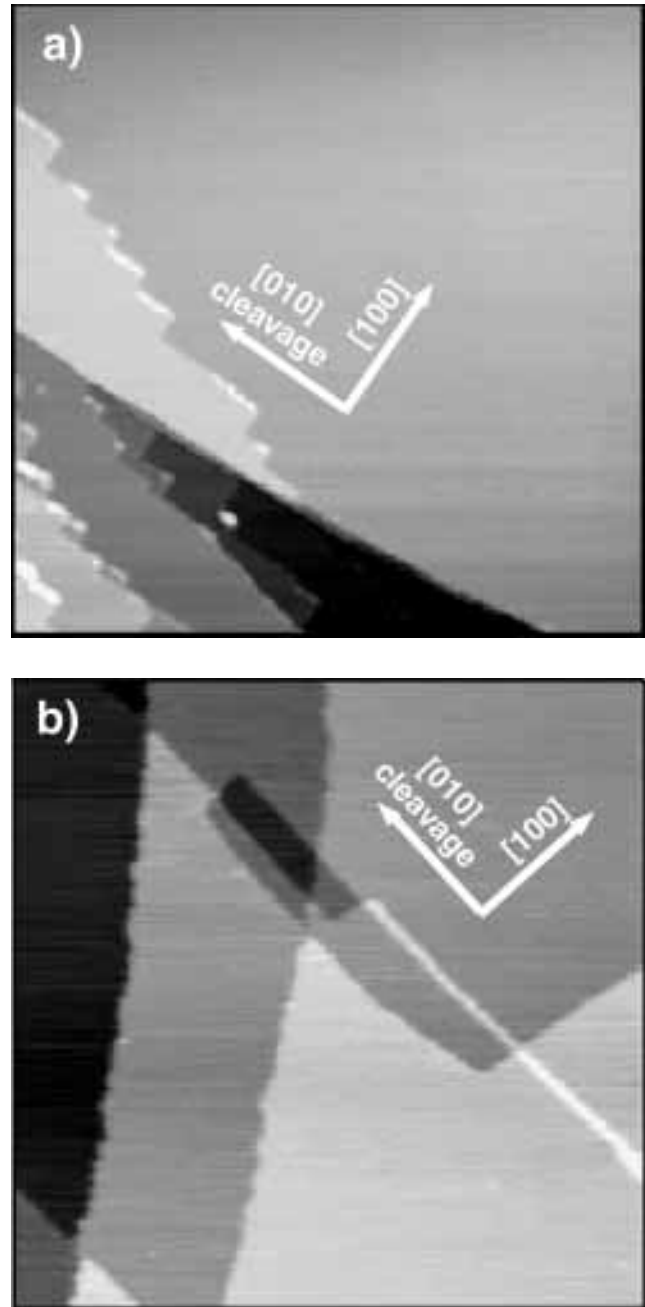


Figure 2. (a) 400×400 nm² topographic image of KCl(001) showing a large flat terrace and several steps in the lower left part of the image. The steps are oriented primarily along the $\langle 100 \rangle$ and $\langle 010 \rangle$ directions. Note the thin bright lines of material present at certain step edges. These structures are 0.32 ± 0.02 nm high, which is equivalent to the KCl step height of 0.315 nm. We believe the bright lines are a narrow strip of KCl. The strips are exclusively present on steps along $\langle 100 \rangle$, which may be a consequence of the cleavage dynamics. (b) 400×400 nm² topographic image of KBr(001). Monatomic steps are seen, some of which cross each other. Some are oriented along low index directions as indicated, although two kinked steps are seen which are not oriented as such.

0.44 ± 0.02 nm for KCl, and 0.49 ± 0.03 nm for KBr. These numbers are based upon an independent calibration of the piezoelectric scanning tubes with respect to the lattice of mica(0001). In all three cases, the stick-slip ex-

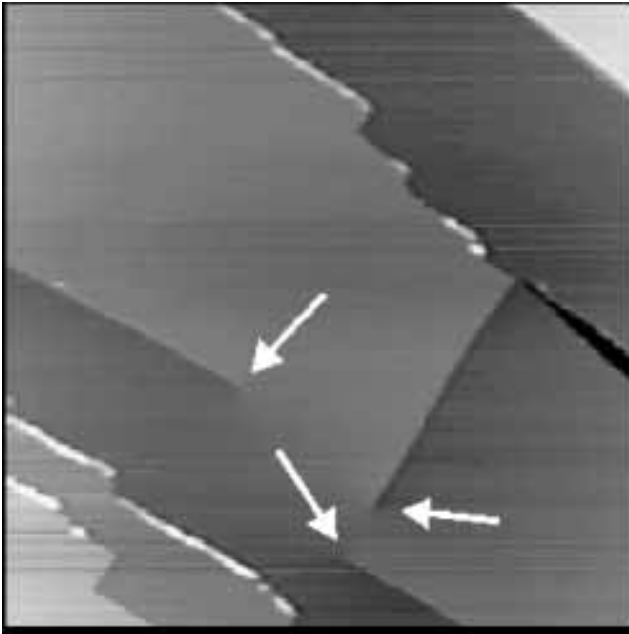


Figure 3. $620 \times 620 \text{ nm}^2$ topographic image of KCl(001). Three screw dislocations are present, with monatomic low index steps emerging from the point where the dislocation line intersects the cleavage surface. This is in agreement with the known Burgers vectors for rock-salt structures [8].

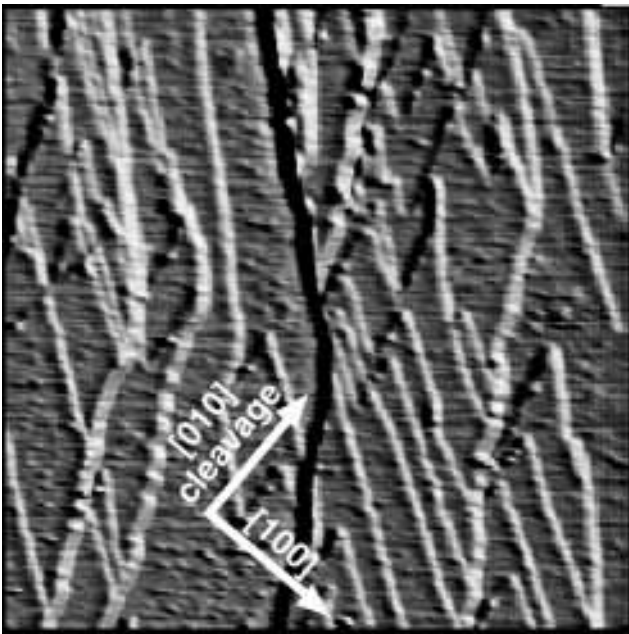


Figure 4. $1.2 \times 1.2 \mu\text{m}^2$ topographic image of KF(001) showing a highly stepped region of the crystal. The image is presented in light-shaded mode to reveal the step structure clearly.

hibits the lattice periodicity d of each material (see table 1 and figure 1). Lattice periodicity is also observed in the simultaneously acquired normal force or topographic images. The stick-slip rows were observed to shift laterally across a monatomic step by half the row spacing, consistent with the rock-salt structure. This was consistently observed over a range of low loads for each material, typically from

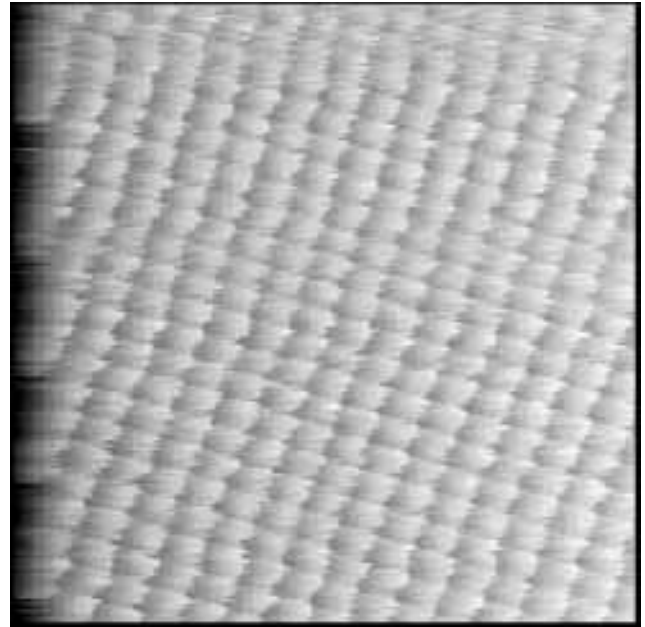


Figure 5. $7.5 \times 7.5 \text{ nm}^2$ lateral force images of KF(001). The periodicity of the lateral force images of all three materials corresponds to d , the periodicity of the lattice (see table 1 and figure 1).

just before the pull-off point to a few nN positive load. At higher positive loads, the contrast tended to reduce.

Therefore, in all cases the stick-slip forces exhibit the lattice periodicity. In the case of KF, this is true in spite of the similar ionic radius of K^+ and F^- ions. Thus, the ionic sites produce unequal contributions to the interfacial potential. This may be due to different relaxations of the ions at the surface [3], or due to the opposite local charge of each site which would interact differently with the tip if it possesses any charge.

4.3. Friction: domains, load dependence

The most remarkable phenomenon observed during these measurements was the repeated appearance of higher friction domains on the terraces which occurred after the tip made contact with the sample, and continued to grow with successive scans. In figure 6, we show an example of this phenomenon on the KBr surface. The topographic image, figure 6(a), shows a number of atomically flat terraces separated by monatomic low index steps. Figure 6(b) is the simultaneously acquired lateral force image. Two distinct friction domains are observed. Some domains are bound by steps, but sometimes their boundary exists on the terrace itself. Most of the boundaries on terraces in this example are oriented roughly perpendicular to the low index steps, i.e., along the [100] direction. The higher lateral force is consistent between both left-to-right and right-to-left scans, therefore the two domains correspond to regions of lower and higher friction force. These differences between the domains are not visible in the topographic image. If any topographic contrast exists between the domains on the KBr surface, it is less than the noise level of 0.02 nm.

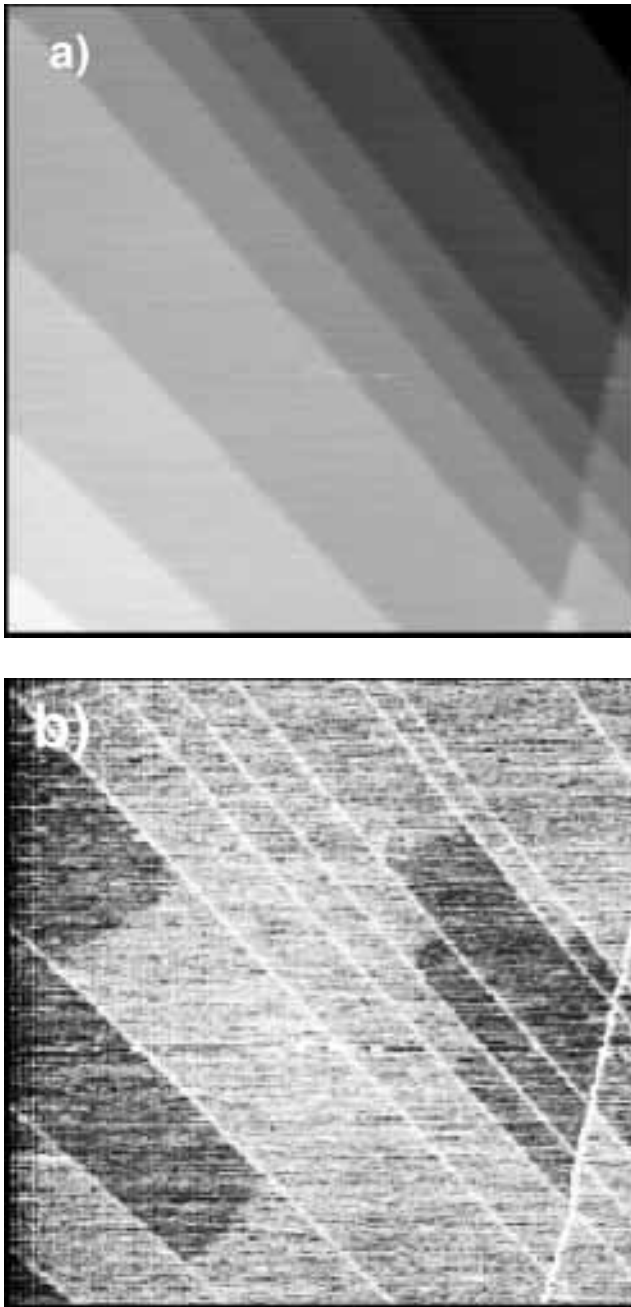


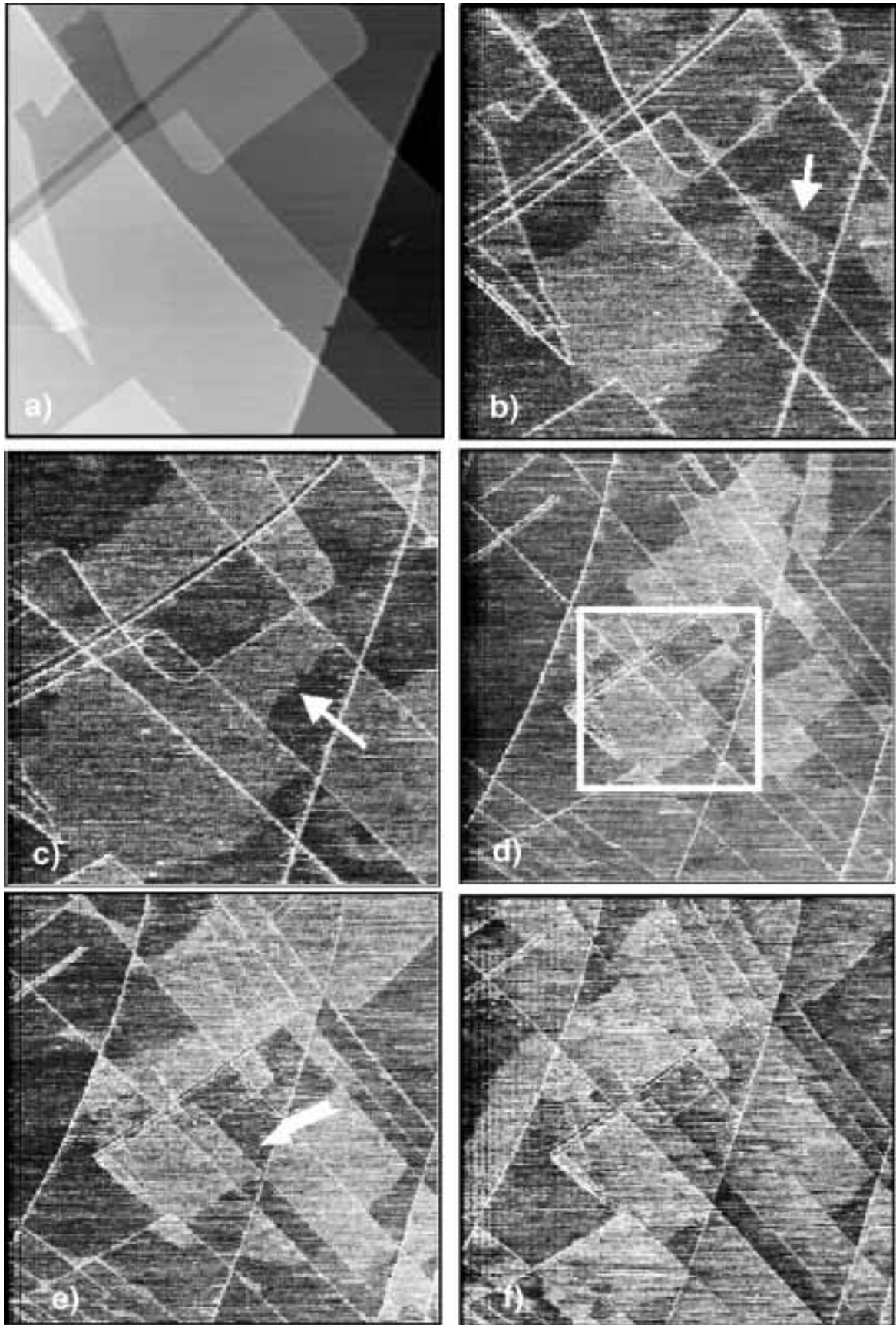
Figure 6. Topographic (a) and simultaneous lateral force (b) images of a $1.2 \times 1.2 \mu\text{m}^2$ region of KBr with a number of low index monatomic steps present. The lateral force image shows clearly resolved domains of low (dark) and high (bright) friction on the terraces. In this example, the domains are sometimes bound by steps but are also bound on terraces themselves perpendicular to the low index steps. There is no apparent topographic contrast corresponding to the friction domains.

The higher friction domains exist within the imaging region and spread between successive scans. This indicates that the low friction domains are associated with the native cleaved surface, while the high friction domains are induced by tip-sample contact. A series of images demonstrating the domain growth is shown in figure 7. Figure 7(a) is a $1.2 \times 1.2 \mu\text{m}^2$ topographic image of the KBr surface in a region with a rather interesting and complicated step

structure. Figure 7(b) is the corresponding lateral force image and figures 7(c)–(f) are subsequent lateral force images (figures 7(d)–(f) are $2.5 \times 2.5 \mu\text{m}^2$ scans, larger than the original scan area). The high friction domains are seen to spread out across terraces and appear to continue outside of the imaging region even though scanning has not occurred there. Some regions remain unaffected even though they are surrounded by high friction domains. Between figures 7(b) and (c) there is a region indicated on a terrace which initially was part of a high friction domain, but has then reverted to a low friction domain while a high friction domain appears elsewhere on the terrace. Later on, in figure 7(e), the entire terrace has reverted to a low friction domain. In this series of images some of the domain boundaries are curved or are not aligned perpendicular to the low-index steps as in figure 6, although some domain boundaries are aligned as such. The average ratio of friction forces between high and low friction domains on the KBr surface is 1.24 ± 0.03 . Often the very first image of a new surface region contains these domains as the tip has already made contact with the surface region during the approach cycle. Since contact is necessary for scanning, it was not possible to determine whether the domain formation was due to contact itself (i.e., normal forces) or scanning (i.e., lateral forces).

Qualitatively similar phenomena were observed on the other samples, but with quantitative differences. An example from the KCl surface is shown in figure 8. The friction contrast is significantly higher (1.79 ± 0.17). This time, there is a small but observable topographic contrast between high and low friction domains of $0.04 \pm 0.02 \text{ nm}$. Like the KBr surface, the high friction domains spread out on terraces from one scan to the next and form several continuous domains, often bound by steps.

As with KBr and KCl, friction domains which spread from one scan to the next appeared on the KF surface as well, but with significantly different properties. The topographic contrast of the domains, $0.20 \pm 0.03 \text{ nm}$, was substantially larger than with KBr and KCl. The friction contrast between domains was also higher, 2.3 ± 0.2 . The lateral domain structure was also distinct. While the high friction domains on KBr and KCl formed connected domains, the high friction domains on KF were generally disconnected. This is illustrated in figure 9. Figures 9(a) and (b) show respectively topographic and lateral force images of a $1.2 \times 1.2 \mu\text{m}^2$ region of KF which includes a step. The topographic contrast of the domains is not far from the KF step height of 0.267 nm . The subsequent lateral force image, figure 9(c), shows that the proportion of surface area converted to high friction domains increases, but the domains are often disconnected or possess rough boundaries. The domain properties for all three materials are summarized in table 2. The domain properties are clearly correlated with the materials' properties as exemplified by the Young's modulus, the anionic radius and the cohesive energy.



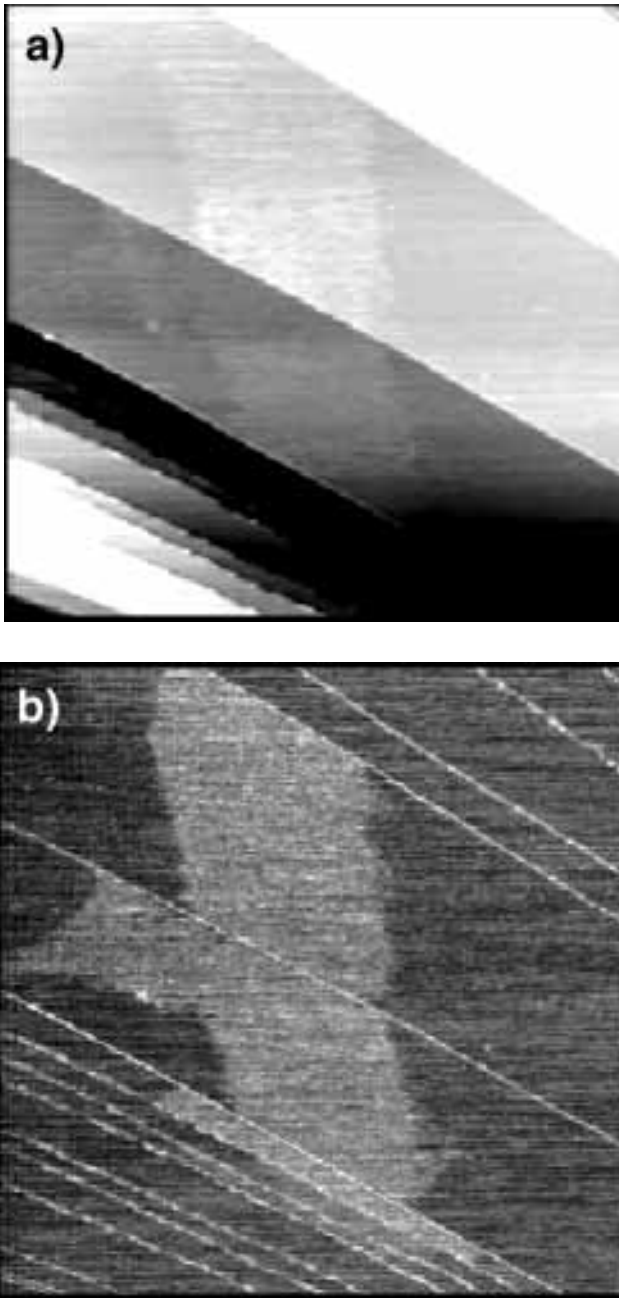


Figure 8. (a) Topographic image of a $1.2 \times 1.2 \mu\text{m}^2$ region of KCl. (b) Simultaneous lateral force image. As with KBr, a connected high friction domain has appeared on some of the terraces. The topographic contrast associated with high friction domains is approximately $0.04 \pm 0.02 \text{ nm}$.

The nature of these domains is striking but mysterious. We know of no previous reports of similar observations. Nor have we observed similar phenomena on UHV

FFM measurements with mica samples. We can rule out the possibility of accumulation of contamination on the surface from the background since the occurrence of domains is always associated with tip-sample contact: after moving from a heavily scanned area where many high friction domains have been created, a newly imaged region will have only a few high friction domains which again increase as scanning/contact proceeds. Therefore, two possibilities occur:

- (1) The domains are produced by contamination transferred from the tip to the sample.
- (2) Tip-sample contact mechanically alters the sample by modifying the organization or density of surface or near-surface atoms. This structural change may involve surface or sub-surface defects such as vacancies or interstitials, or relative motion causing misfit or misalignment of near surface layers, and is produced by the substantial stresses present around the tip-sample contact zone.

The results we have obtained are not conclusive enough, nor is the present day understanding of nanometer scale tribology comprehensive enough, to allow us to categorically confirm either of these possibilities. However, several factors favor the second explanation. Although there is some observable shifting of the domain boundaries, once they are formed they are generally maintained. There is no sign of destruction of a layer of contamination by the tip. For example, no domains were observed to have boundaries or modifications along the scan direction. Yet one might expect to be able to modify a contamination or adsorbate layer with the tip, as observed for example by Lüthi et al. in the case of C_{60} and AgBr monolayer islands on NaCl on UHV [27]. Repeated attempts at this were unsuccessful. At very high loads, the tip gouged through the surface producing a hole. This will be discussed further below. It was not possible to alter a high friction domain without altering the substrate itself. Therefore, if the high friction domains are a contamination layer then they are very strongly bound to the substrate. It is surprising that material which could readily transfer from the tip to the substrate could then be strongly bound to the substrate especially considering the inert quality of alkali halide surfaces.

No reduction in the rate of domain formation was observed during the experiment. If contamination from the tip occurred, then the source was never depleted during the course of the experiment, which was 14 days of data acquisition involving over 400 images. It seems surprising that tip contamination could persist for such a duration, whereas surface alteration obviously would occur steadily.

Figure 7. (Left.) (a) $1.2 \times 1.2 \mu\text{m}^2$ topographic image of KBr. (b) Simultaneous lateral force image. (c)–(f) Subsequent lateral force images: (c) 2nd scan; (d) 3rd scan; (e) 6th scan; (f) 13th scan. Note that (d)–(f) are $2.5 \times 2.5 \mu\text{m}^2$ images of the same region, with the original imaging region from (a) indicated by the white box. There is some lateral drift between images. High friction domains grow from one scan to the next. The terrace indicated by the arrow in (b) initially has a high friction domain covering part of it which reverts to low friction (c)–(d) while another part of the terrace is converted to a high friction domain. Later, the entire terrace reverts to low friction again (e). Most of the other high friction domains remain once formed. Domains appear to grow beyond the scan area.

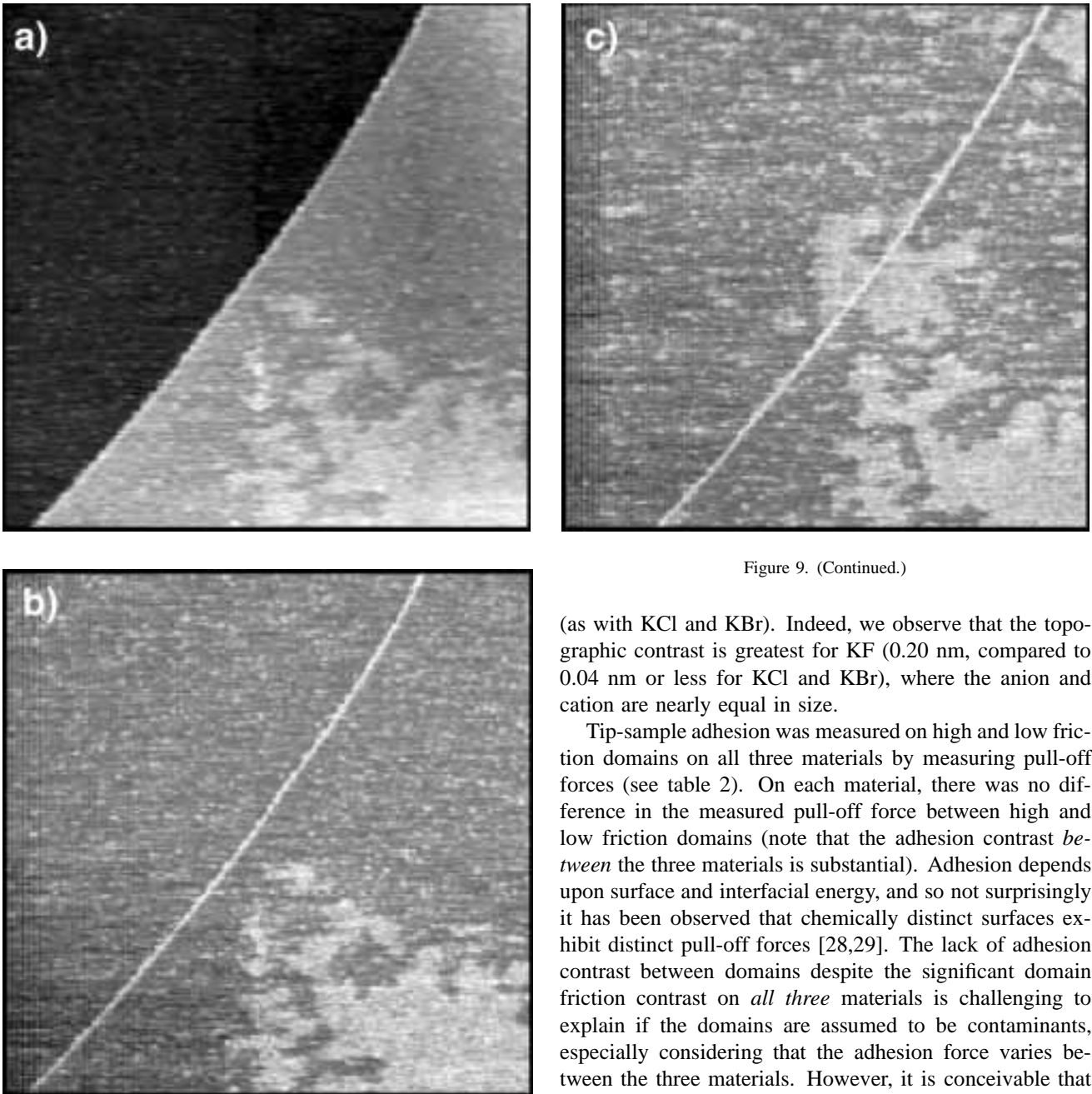


Figure 9. (Continued.)

Figure 9. (a) Topographic image of a $1.2 \times 1.2 \mu\text{m}^2$ region of KF. (b) Simultaneous lateral force image. (c) Subsequent lateral force image, 4 scans later. High friction domains grow from one scan to the next. The topographic contrast of the domains is approximately $0.20 \pm 0.03 \text{ nm}$. The domains are more disconnected than with KBr and KCl and have rougher boundaries.

Furthermore, it is peculiar for a contamination layer to exhibit different topographic contrast on the different materials. However, it is conceivable that the topographic properties of surface structures associated with defects or dislocations ought to vary with the type of material. Let us assume that interstitial creation is occurring. Packing ions into interstitial positions when the neighbors are of the same size (as with KF) must distort the neighboring ions to a greater degree than packing a much smaller ion would

(as with KCl and KBr). Indeed, we observe that the topographic contrast is greatest for KF (0.20 nm, compared to 0.04 nm or less for KCl and KBr), where the anion and cation are nearly equal in size.

Tip-sample adhesion was measured on high and low friction domains on all three materials by measuring pull-off forces (see table 2). On each material, there was no difference in the measured pull-off force between high and low friction domains (note that the adhesion contrast *between* the three materials is substantial). Adhesion depends upon surface and interfacial energy, and so not surprisingly it has been observed that chemically distinct surfaces exhibit distinct pull-off forces [28,29]. The lack of adhesion contrast between domains despite the significant domain friction contrast on *all three* materials is challenging to explain if the domains are assumed to be contaminants, especially considering that the adhesion force varies between the three materials. However, it is conceivable that *structurally* distinct domains would not produce significant adhesion contrast. Although it is not known exactly how adhesion depends upon atomic structure, adhesion may not be strongly affected by atomic scale roughening or disorder as it may be determined by electrostatic or van der Waals forces whose effect goes beyond the surface layer. On the other hand, atomic scale roughening could strongly affect friction by presenting a “bumpy path” which the tip needs to traverse. Furthermore, the presence of defects provides a number of new vibrational modes for energy dissipation, particularly soft modes associated with vacancies and interstitials which allow facile atom displacement.

Figure 7 shows that some terraces remain unaffected while high friction domains have been created on neighboring terraces. It would be surprising that contamination would so strongly favor a particular terrace for growth while

Table 2
Properties of friction domains.

Sample	Anion radius (nm)	Young's modulus (GPa)	Domain height (nm)	Adhesion – high friction domain (nN)	Adhesion – low friction domain (nN)	Domain friction contrast (hi : lo)	Lateral structure
KF	0.136	60	0.20 ± 0.03	4.6 ± 0.5	4.7 ± 0.6	2.3 ± 0.2	Disconnected
KCl	0.181	39	0.04 ± 0.02	2.7 ± 0.5	2.9 ± 0.4	1.79 ± 0.17	Connected
KBr	0.195	33	< 0.02	3.2 ± 0.3	3.4 ± 0.2	1.24 ± 0.03	Connected

completely avoiding a neighboring terrace. Furthermore, as seen in figure 8, a large domain can appear from one image to the next and then remain the same size. Again this behavior would be hard to understand if contamination were involved since a more uniform increase in the affected area would be expected. However, a modified surface structure could conceivably be dependent on the initial presence of defects which would not be equal amongst terraces, and which could determine the boundaries of the domains.

The domains often appear to grow from step edges themselves. This can be seen in figure 8, as well as figure 10, which clearly shows domains originating from step corners, i.e., from dislocation intersections. These would be the most highly stressed regions of the surface. The domains may in fact be a stress relief mechanism initiated by tip contact.

The creation of surface damage that is not apparent in AFM topography is consistent with previous results by Hu et al. with mica substrates [30]. In that work, a single scan at a high applied load could produce a monolayer deep hole in the mica sample. A single scan at an intermediate load produced no such hole and no apparent topographic effects. Repeated scans over the same area at these intermediate loads were similar to the first until suddenly the surface ruptured and once again a monolayer deep hole was produced on the surface. Multiple scans at lower loads produced no hole at all, even after hundreds of repetitions. This strongly suggests that at the intermediate load regime, defects which were imperceptible in topographic scans must have been accumulating, leading to eventual surface damage on a larger scale. Furthermore, the absence of this effect in the lowest load regime suggests a threshold for defect creation. Mica exhibits strong lateral covalent bonding within a molecular layer, and these layers are bound together by electrostatic forces. To produce a hole, the covalent bonds within a layer must be ruptured. In the present case, we found that domain formation was unavoidable even if the lowest possible loads were utilized. This may not be so surprising since these alkali halides are less strongly bound than the covalently bound species of mica. Furthermore, our tip was relatively sharp, ensuring substantial contact stresses.

Using the JKR contact mechanics theory [31], we can perform rough estimates of the compressive stresses that would be present in the contact zone. These calculations utilize the tip radius measurement described above, and bulk values of the elastic constants for the tip and sample materials. For example, in the case of KCl with zero exter-

nally applied load, we estimate an average contact pressure of 180 MPa, and a maximum contact pressure of 720 MPa at the contact zone center. For KF, the corresponding estimates are 250 MPa average pressure, and 1.0 GPa maximum pressure. A substantial fraction of the total stress is comprised by shear stress which is the component that generally leads to wear. The maximum pressures are close to or within the range of the materials' ideal yield strengths (see table 1). Furthermore, short-range adhesion, which is likely in UHV, contributes to high tensile stresses at the contact zone edge [31,32]. Shear stresses due to tip-sample friction will be comparable in magnitude and will add to the total stress. Surface alteration due to any these stresses is therefore feasible.

We can also estimate, very roughly, the energy dissipated by friction and compare that to defect formation energies. Using KCl as an example, the average force relaxation observed for a single atomic stick-slip event is 2.0 ± 0.3 nN, measured at zero applied load. This corresponds to 5.5 eV of energy dissipated. For lack of any better comparison, the bulk formation energy of a Frenkel defect (vacancy-interstitial pair) is estimated to be in the range of 3.2–3.6 eV for a cation interstitial, and 3.4–4.4 eV for an anion interstitial [33]. Thus, there is more than enough energy dissipated in a *single* stick-slip event for a Frenkel defect to be created. At zero applied load, the JKR theory predicts a contact area of 16 nm², which is about 82 KCl unit cells. If the tip is scanned laterally by one contact radius, enough energy has been dissipated to create 8.3 defects, or roughly 10% of the sites within the contact zone. This is for *one* line scan; an area scan would consist of multiple line scans which could create many defects. Of course, much of the energy could be dissipated through phonon excitation or other ways. Nevertheless, significant defect formation is not out of the question. Therefore, both frictional interactions and the substantial stresses present in the contact zone could alter surface and near-surface atoms.

Experimental work by Wilson and Williams [34] demonstrates that surface damage can be assisted by tip-sample contact for the case of an alkali halide. They examined the potassium iodide (KI) surface using AFM while exposing the sample *in situ* to UV light. The UV light creates surface and near-surface defects by electronically induced desorption of halogen ions. While the measurements were not carried out in UHV, the relative humidity was kept around 15%, low enough to eliminate most wear effects attributable to humidity. While the UV light created surface

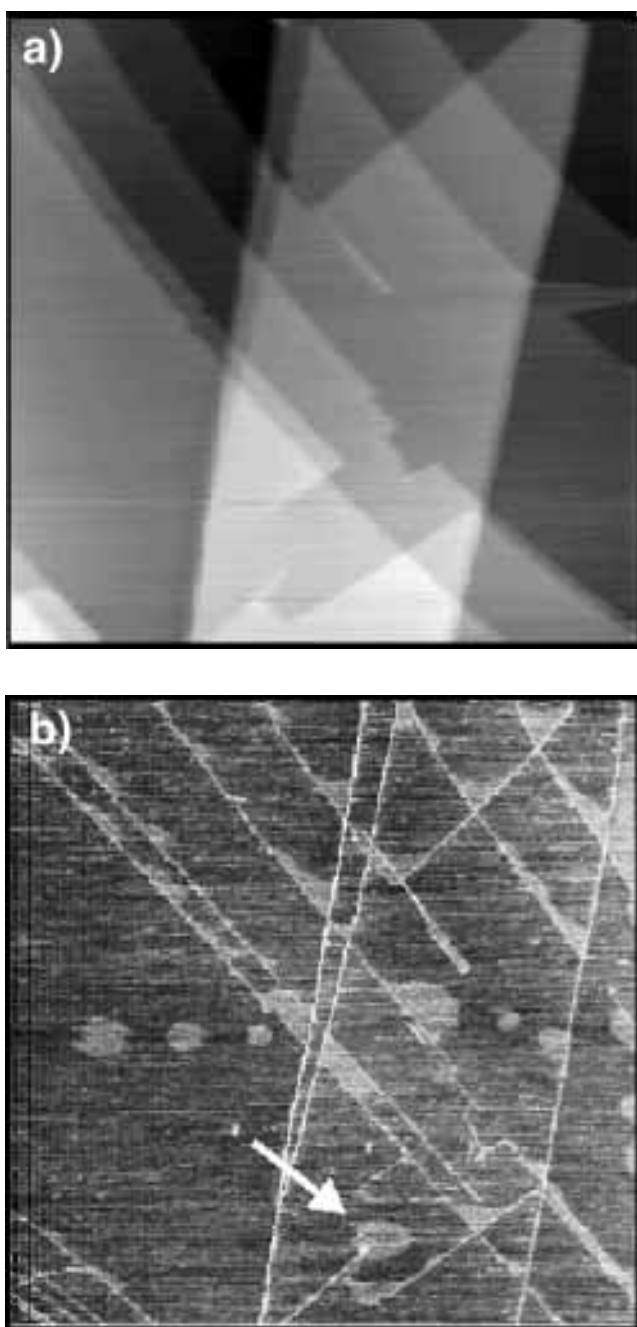


Figure 10. (a) Topographic image of a $2.5 \times 2.5 \mu\text{m}^2$ region of KBr. (b) Subsequent lateral force image. High friction domains grow from step edges as well as corners where steps cross, and sharp kinks in steps (indicated by the arrow). The series of round domains across the middle of the image corresponds to where a series of horizontal line scans were performed prior to acquiring the images.

damage on its own, regions that were scanned by the tip during UV light exposure showed significantly enhanced damage compared to neighboring regions that were not scanned during UV exposure. The authors therefore concluded that the damage was accelerated by “tip agitation”. It is clear from this example that substantial structural modification was accelerated by tip-sample contact, at a load of around 10 nN.

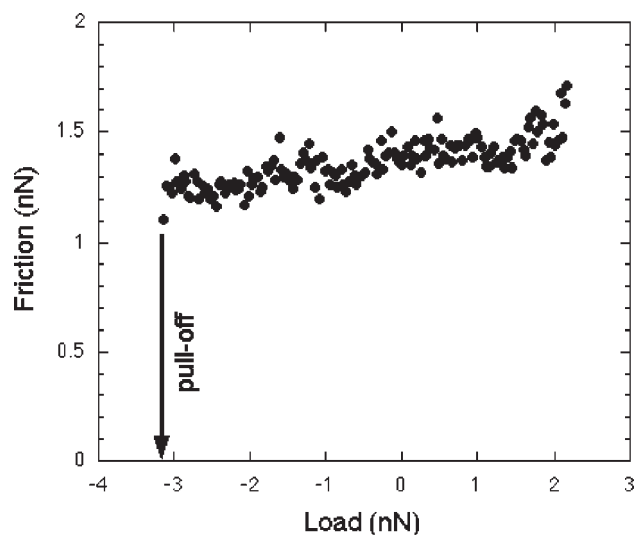


Figure 11. Friction vs. load plot for KBr within a low load regime. There is a significant finite friction force at the pull-off point, and the friction only has a weak, nearly linear dependence upon load. This is unlike previous measurements of friction vs. load on other materials which corresponded to elastic behavior.

The theoretical work of Shluger et al. concerning the creation of defects by AFM on alkali halides [35,36] is relevant here. These authors simulated the AFM scanning process using a zero-temperature static atomistic technique for a hard, sharp ionic MgO tip scanning a NaCl sample. In their simulations they found that under moderate loading conditions, transfer of ions from sample to tip and creation of Frenkel defects occurred frequently. In their simulation, these processes could be avoided at low loads with an inert tip, but were unavoidable at higher loads and with a less inert (i.e., a charged) tip. In addition, these processes frequently reversed, i.e., the interstitial atom relaxed back into the vacancy position. However, their simulation involved a very sharp tip (the corner of a $(\text{MgO})_{32}$ cube). More complex behavior would be anticipated for the larger contact area present under experimental conditions. The ease with which defects were created in these simulations suggest that substantial defect formation in actual experimental conditions is plausible.

The connected form of the domains on KCl and KBr and their interaction with steps, as well as the uniformity of the friction force on the high friction domains for each material, suggests a uniform nature that involves some kind of lateral interaction within a domain. It is possible that the domains are regions of enhanced surface relaxation, or regions of the surface layer that are slipped or displaced with respect to the layer below. Materials are highly strained in the neighborhood of dislocations. Thus, the electrostatic energy cost of such a rearrangement could be paid for by the reduction of strain which is associated with dislocations. The presence of a surface itself is known to allow relaxation of strain near dislocations [8]. However, it is difficult to propose specific mechanisms since so little is known about defects and dislocation properties at surfaces of ionic materials. At the very least we can state that the domains

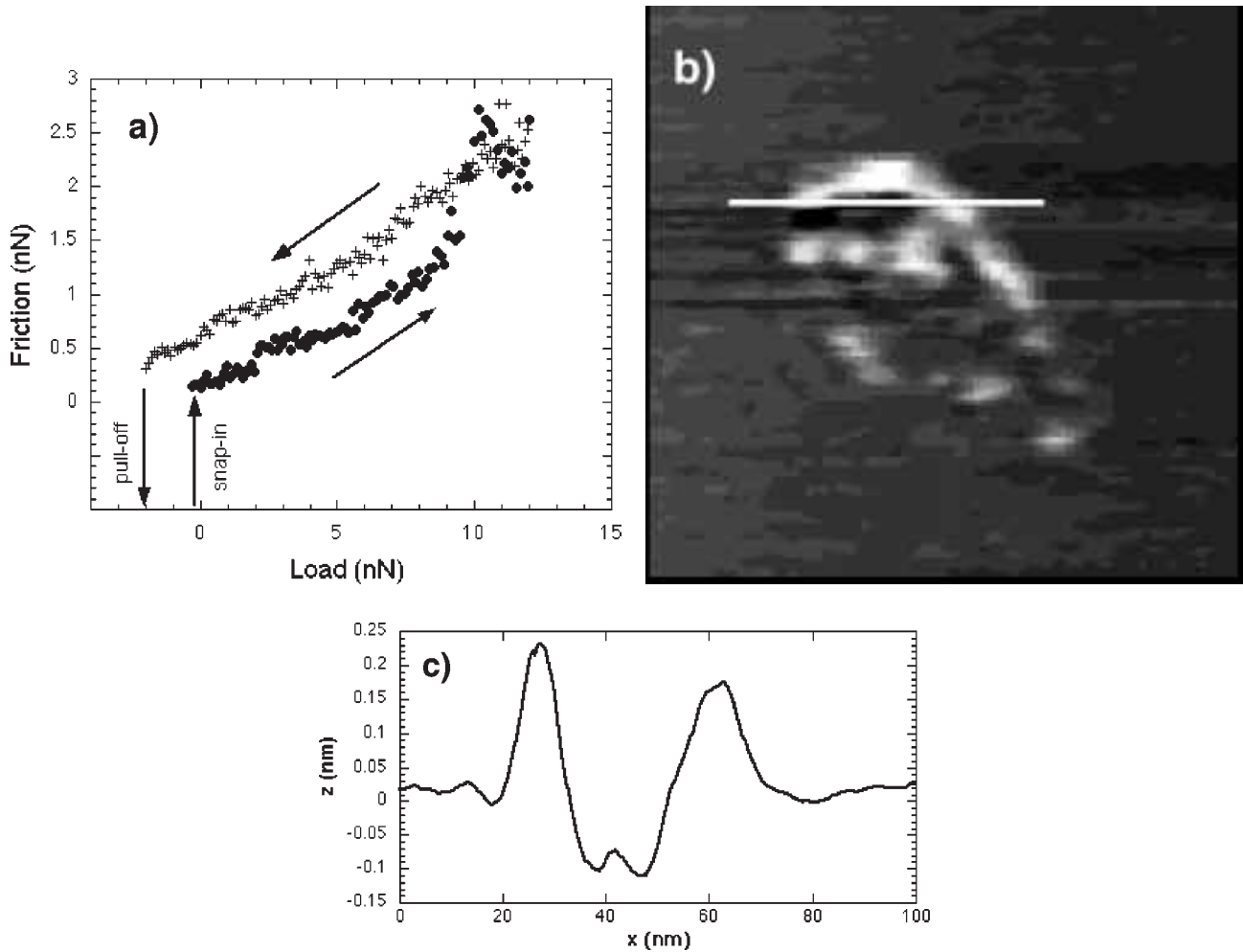


Figure 12. (a) Friction vs. load plot for KCl for a wide load regime. Friction increases gradually with load until about 5.5 nN where the increase is more rapid. At 9 nN, the increase is dramatic and is followed by a fluctuation of the friction force. Upon retraction, friction does not recover to original values. (b) Topographic image of the region scanned in part (a). A line has been gouged in the sample with material piled up at the sides. (c) A line profile of the gouged area.

appear to be structurally, but not chemically distinct from one another, either in their organization or density.

Friction vs. load measurements were acquired on all three materials. Previous measurements of the load dependence of friction on mica [24,25] and other materials [37] indicate that, at low loads, the friction force is proportional to the contact area predicted by continuum mechanics theories. However, for the present experiments, no such proportionality was obtained. Furthermore, it was found that the load dependence of friction was generally not reproducible from one measurement to the next. The lack of correlation with continuum mechanics models of elastic contacts suggests that the tip-sample contacts are not elastic in these cases. However, some features of the friction forces were reproducible. An example from the KBr surface is shown in figure 11. The common feature of all the friction measurements on these materials is that some finite shear force exists even at the lowest loads, and that only a modest increase of friction with load is observed for the low-load regime. This example shows an apparently linear dependence of friction upon load, although other measurements

displayed a small non-linear component. The value of the friction force at the pull-off point varied significantly from one measurement to the next but was typically between 0.3 and 1.5 nN for all three materials. Finite friction at low loads in elastic contacts is due to short range adhesion that produces a finite contact area, but in this case may also be related to energy dissipation by surface modification.

Friction vs. load measurements can be acquired for higher load ranges and exhibit distinct behavior characteristic of larger scale wear. An example from the KCl surface is shown in figure 12. The experiment begins with the tip out of contact with the sample. At the indicated snap-in point, finite friction is observed which initially increases gradually with load. In this example, above 9 nN the rate of increase becomes substantially greater. Eventually friction actually reduces with increasing load. Upon retraction, significant hysteresis is observed. An image of the scan region reveals the creation of a hole approximately one atomic layer deep (figures 12(b), (c)), with material piled up at the sides. We believe that the region of steep increase of friction with load is associated with the actual gouging process. The

reduction of friction with load at high loads may be associated with the completion of removal of the first layer of material. These measurements clearly represent a more advanced stage of wear than the domain formation described above and will be studied in further detail in the future.

5. Summary

We have measured surface properties of KF, KCl and KBr(001) surfaces in UHV using contact mode AFM. UHV cleavage produces atomically flat terraces with stable monatomic step structures. Atomic lattice resolution images have been acquired on all three surfaces which exhibit the lattice periodicity of each of the materials. We have observed a new phenomenon where tip-sample contact induces higher friction domains.

While the observations are not entirely conclusive regarding the nature of the observed friction domains, the evidence suggests that defect formation is involved. This is an interesting phenomenon to study since it has implications for our understanding of the initial stages of wear and the ability of AFM to measure it. Specifically, these observations indicate that domains of surface or near-surface defects can be created by tip-sample contacts. Furthermore, the presence of defects is manifested in both the magnitude and load dependence of the friction force. This suggests an important and observable relationship between defects and energy dissipation. Future experiments will attempt to elucidate the mechanism of domain creation and determine their exact structure and properties.

Acknowledgement

We would like to thank Drs. L. Xu, F. Rieutord and H. Bluhm for useful discussions. RWC acknowledges support from the Natural Sciences and Engineering Research Council of Canada. This work was supported by the Director, Office of Energy Research, Basic Energy Sciences, Materials Sciences Division of the US Department of Energy under contract DE-AC03-76SF00098.

References

- [1] G. Binnig, C.F. Quate and C. Gerber, *Phys. Rev. Lett.* 56 (1986) 930.
- [2] R.W. Carpick and M. Salmeron, *Chem. Rev.* 97 (1997) 1163.
- [3] A.M. Stoneham, *Cryst. Lattice Defects Amorph. Mater.* 14 (1987) 173.
- [4] L. Pauling, *The Nature of the Chemical Bond and the Structure of Molecules and Crystals; an Introduction to Modern Structural Chemistry* (Cornell University Press, Ithaca, NY, 1960).
- [5] M.P. Tosi, in: *Solid State Physics*, Vol. 16, eds. F. Seitz and D. Turnbull (Academic Press, New York, 1964).
- [6] G. Simmons and H. Wang, *Single Crystal Elastic Constants and Calculated Aggregate Properties: a Handbook* (MIT Press, Cambridge, MA, 1971).
- [7] A. Kelly, *Strong Solids* (Oxford University Press, London, 1973).
- [8] M.T. Sprackling, *The Plastic Deformation of Simple Ionic Crystals* (Academic Press, London, 1976).
- [9] N. Agraït, G. Rubio and S. Vieira, *Phys. Rev. Lett.* 74 (1995) 3995.
- [10] S. Morita, S. Fujisawa and Y. Sugawara, *Surf. Sci. Rep.* 23 (1996) 3.
- [11] D.F. Ogletree, R.W. Carpick and M. Salmeron, in preparation (1997).
- [12] L. Howald, R. Lüthi, E. Meyer, G. Gerth, H. Haefke, R. Overney and H.J. Güntherodt, *J. Vac. Sci. Technol. B* 12 (1994) 2227.
- [13] R. Lüthi, E. Meyer, M. Bammerlin, L. Howald, H. Haefke, T. Lehmann, C. Loppacher, H.J. Güntherodt, T. Gyalog and H. Thomas, *J. Vac. Sci. Technol. B* 14 (1996) 1280.
- [14] S. Fujisawa, Y. Sugawara and S. Morita, *Philos. Mag. A, Phys. Condens. Matter Struct. Defects Mech. Prop.* 74 (1996) 1329.
- [15] J.B. Pethica and A.P. Sutton, *J. Vac. Sci. Technol. A* 6 (1988) 2494.
- [16] F.J. Giessibl, *Science* 267 (1995) 68.
- [17] M. Bammerlin, R. Lüthi, E. Meyer, A. Baratoff, J. Lü, M. Guggisberg, C. Gerber, L. Howald, H. Haefke and H.J. Güntherodt, *Probe Microscopy 1* (1997) 3.
- [18] Optovac, North Brookfield, MA.
- [19] Prof. M. DeLong, Dept. of Physics, University of Utah.
- [20] Sharpened Microlever type E, Park Scientific Instruments, Sunnyvale, CA.
- [21] D.F. Ogletree, R.W. Carpick and M. Salmeron, *Rev. Sci. Instrum.* 67 (1996) 3298.
- [22] Q. Dai, R. Vollmer, R.W. Carpick, D.F. Ogletree and M. Salmeron, *Rev. Sci. Instrum.* 66 (1995) 5266.
- [23] S.S. Sheiko, M. Möller, E.M.C.M. Reuvekamp and H.W. Zandbergen, *Phys. Rev. B* 48 (1993) 5675.
- [24] R.W. Carpick, N. Agraït, D.F. Ogletree and M. Salmeron, *J. Vac. Sci. Technol. B* 14 (1996) 1289.
- [25] R.W. Carpick, N. Agraït, D.F. Ogletree and M. Salmeron, *Langmuir* 12 (1996) 3334.
- [26] M. Luna, N.A. Melman, F. Rieutord, Q. Dai, D.F. Ogletree and M. Salmeron, *J. Phys. Chem.* (1997), submitted.
- [27] R. Lüthi, E. Meyer, H. Haefke, L. Howald, W. Gutmannsbauer, M. Guggisberg, M. Bammerlin and H.J. Güntherodt, *Surf. Sci.* 338 (1995) 247.
- [28] C.D. Frisbie, L.F. Rozsnyai, A. Noy, M.S. Wrighton and C.M. Lieber, *Science* 265 (1994) 2071.
- [29] J.N. Israelachvili, *Intermolecular and Surface Forces* (Academic Press, London, 1992).
- [30] J. Hu, X.D. Xiao, D.F. Ogletree and M. Salmeron, *Surf. Sci.* 327 (1995) 358.
- [31] K.L. Johnson, K. Kendall and A.D. Roberts, *Proc. Roy. Soc. Lond. A* 324 (1971) 301.
- [32] D. Maugis, *J. Colloid Interface Sci.* 150 (1992) 243.
- [33] D.K. Rowell and M.J.L. Sangster, *J. Phys. C (Sol. State Phys.)* 14 (1981) 2909.
- [34] R.M. Wilson and R.T. Williams, *Nucl. Instrum. Methods Phys. Res.* 101 (1995) 122.
- [35] A.L. Shluger, R.T. Williams and A.L. Rohl, *Surf. Sci.* 343 (1995) 273.
- [36] A.L. Shluger, A.L. Rohl, R.T. Williams and R.M. Wilson, *Phys. Rev. B* 52 (1995) 11398.
- [37] E. Meyer, R. Lüthi, L. Howald, M. Bammerlin, M. Guggisberg and H.J. Güntherodt, *J. Vac. Sci. Technol. B* 14 (1996) 1285.